nature communications

Article

https://doi.org/10.1038/s41467-025-57227-5

Ephemeral superconductivity atop the false vacuum

Received: 11 September 2024

Accepted: 12 February 2025

Published online: 27 February 2025

Check for updates

Gal Shavit[1,2] ✉, Stevan Nadj-Perge[1,3] & Gil Refael[1]

A many-body system in the vicinity of a first-order phase transition may get trapped in a local minimum of the free energy landscape. These so-called false-vacuum states may survive for exceedingly long times if the barrier for their decay is high enough. The rich phase diagram obtained in graphene multilayer devices presents a unique opportunity to explore transient superconductivity on top of a correlated false vacuum. Specifically, we consider superconductors which are terminated by an apparent first-order phase transition to a correlated phase with different symmetry. We propose that quenching across this transition leads to a non-equilibrium ephemeral superconductor, readily detectable using straightforward transport measurements. Moreover, the transient superconductor also generically enhances the false vacuum lifetime, potentially by orders of magnitude. In several scenarios, the complimentary effect takes place as well: superconductivity is temporarily emboldened in the false vacuum, albeit ultimately decaying. We demonstrate the applicability of these claims for different instances of superconductivity terminated by a first order transition in rhombohedral graphene. The obtained decay timescales position this class of materials as a promising playground to unambiguously realize and measure non-equilibrium superconductivity.

Phase transitions in many-body correlated systems may often be succinctly described by an appropriate classical or quantum field theory[1,2]. The equilibrium many-body ground state is identified by the global minimum of the free energy associated with this description. However, other locally stable minima may exist, albeit with a higher energy density.

These minima act as the "false-vacuum" (FV) of the system and may be long-lived due to their metastable nature. A system can generically get trapped in the FV state when it is quenched through a first-order phase transition. Supercooling and superheating of water are well-known classical examples of this phenomenon[3], yet quantum systems such as spin chains[4–6], superconducting wires[7], and atomic superfluids[8] have been show to exhibit metastable phases and FV decay. Further, the FV concept itself has originated in the context of cosmology, where it may have truly dire implications[9–11].

In recent years, graphene multilayers have emerged as an exciting platform with a high degree of tunability to study correlated electron phenomena, topological phases, unusual superconductivity, and their interplay[12–34]. A recurring theme in these systems is the peculiar vicinity of the superconducting phases to symmetry-breaking phase transitions. In several cases, the superconducting dome itself is terminated by an abrupt transition where the Fermi surface undergoes significant reconstruction[23,24,26–28,30,35,36], which in some instances is strongly indicative of a first-order phase transition[37–39]. Recently, similar phenomenology was observed in twisted bilayer WSe_2, where hysteretic behavior was observed at the boundary between superconductivity and a correlated phase[40].

In this work, we propose these materials as a platform for realizing and exploring out-of-equilibrium superconductivity, which exists as a metastable phase on top of the FV manifold of the symmetry-broken phase.

[1]Department of Physics and Institute for Quantum Information and Matter, California Institute of Technology, Pasadena, California, USA. [2]Walter Burke Institute of Theoretical Physics, California Institute of Technology, Pasadena, California, USA. [3]T. J. Watson Laboratory of Applied Physics, California Institute of Technology, Pasadena, California, USA. ✉e-mail: gshavit@caltech.edu

This extraordinary non-equilibrium metastable state arises in the vicinity of the true vacuum symmetry-broken phase. A useful heuristic of the sort of scenarios we discuss is presented in Fig. 1. In this generic phase diagram, superconductivity and a correlated phase are in close proximity, separated by a first-order transition line. Specifically, we are interested in cases where the correlated phase preempts superconductivity and overtakes it. Thus, after a sudden quench from the superconducting phase across the transition (black arrow in Fig. 1), there exists a possibility of a long-lived transient superconductor, realized on top of the FV. Alternatively, we also consider quenching from a parent normal phase directly into the suppressed superconductor through a first-order transition (green arrow). Such a protocol may allow one to reveal buried underlying superconductivity in such systems, masked by competing phases.

We underline the regimes where FV superconductivity are most relevant and experimentally accessible. This is accomplished by combining microscopic calculations for two candidate materials, rhombohedral trilayer graphene (RTG) and Bernal-stacked bilayer graphene (BBG), and a field theoretical description of the FV decay phenomena. We estimate the expected lifetimes of the ephemeral superconductors to be of the order of ~100 nanoseconds, enabling straightforward detection methods relying on time-resolved transport measurements. Remarkably, the unusual presence of superconductivity in the FV state is what *enables* such simplified detection schemes in a solid-state setting. Superconductivity provides an unambiguous transport signal – a delay between a current driven through the system and the appearance of a voltage drop.

Furthermore, we show that the incompatibility between the correlated symmetry-broken phase and the superconductor *non-trivially enhances the stability of the FV and its lifetime*. As we show, this is a generic feature in scenarios where a subordinate phase develops on top of a "primary" false vacuum. This may be understood as a result of the magnification of the surface tension between the true and false vacuum states of the system. The strength of surface tension plays a major role in determining the energetics of the FV decay.

Interestingly, the FV superconductivity may actually survive at higher temperatures compared to its equilibrium counterpart on the other side of the transition. This transient enhancement of superconductivity comes at the cost of incurring a finite lifetime. Generically, what drives the symmetry-breaking transition which terminates the superconductor is the density of states (DOS) near the Fermi level ν. Clearly, it is also an important factor in the determination of the superconducting properties. For example, conventionally the superconducting transition temperature $T_c \propto \exp\left(-\frac{1}{u\nu}\right)$ (u is the pairing strength). For weak-coupling superconductors, $u\nu \ll 1$, T_c is especially sensitive to ν. In the FV, the superconductor temporarily experiences a higher DOS while the correlated phase is suppressed. This facilitates favorable superconducting properties, potentially beyond those available at equilibrium under similar conditions.

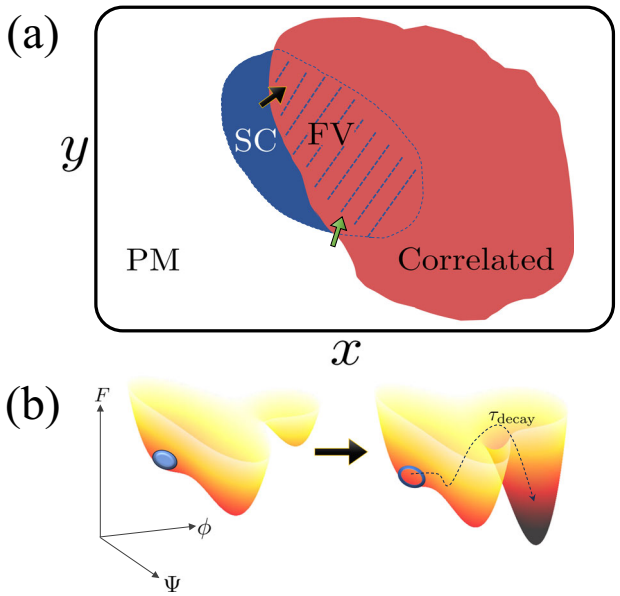

Fig. 1 | Schematic equilibrium phase diagram hosting ephemeral superconductivity. a As a function of tuning parameters (x, y) a superconducting region exists (SC, blue), surrounded by a parent "normal" state (PM, white) and a symmetry-broken correlated phase (red). The correlated phase suppresses an otherwise superconducting region in parameter space (hatched red-blue). Here, we consider a quench across a first-order transition boundary to the FV superconductor, either directly from an equilibrium superconducting phase (black arrow) or from the normal state (green arrow). **b** Illustration of the energy landscape as a function of the two order parameters ϕ, Ψ across the transition. In the equilibrium superconducting phase (left) Ψ is condensed (blue ellipse). Following the quench (black arrow), the new equilibrium state has ϕ condensation and zero superconductivity. The ephemeral superconductor (empty ellipse) has a finite lifetime of ~ τ_{decay} before decaying to the true vacuum (via the dashed line trajectory).

Results

False vacuum decay

We consider scenarios where as a function of some tuning parameter, r (which can be a magnetic field, an electric displacement field, pressure, etc.), a system undergoes a first-order phase transition with an order parameter $\hat{\phi}$. Within this $\hat{\phi}$-ordered phase, it is further assumed that the disordered (e.g., paramagnetic) phase remains a metastable local minimum of the effective free energy.

Let us also examine the consequences of an additional phase, with order parameter $\hat{\Psi}$, which (i) also condenses in the vicinity of the $\hat{\phi}$ phase transition, and (ii) is *incompatible* with the $\hat{\phi}$ phase. Generally, we will be interested in the case where the energy scales associated with $\hat{\phi}$ dominate over those of $\hat{\Psi}$, and the $\hat{\phi}$ order is the equilibrium ground state, and the so-called "true vacuum".

The scenario we describe above may be captured by the following Ginzburg-Landau free energy functional,

$$\begin{aligned} F = &\int d^2x \left[\frac{\sigma}{2}|\nabla\phi|^2 + 16g\phi^2(\phi-1)^2 - B\phi^2\right] \\ &+ \int d^2x \left[\frac{\kappa}{2}|\nabla\Psi|^2 - \frac{a(r)}{2}|\Psi|^2 + \frac{b}{4}|\Psi|^4\right] \\ &+ \frac{\lambda}{2}\int d^2x |\Psi|^2\phi^2. \end{aligned} \tag{1}$$

Clearly, the first-order transition is governed by the parameter denoted as B. When $B<0$, $\phi=0$ (the paramagnetic phase where the spontaneous ordering of $\hat{\phi}$ does not yet occur) minimizes the free energy in the absence of $\hat{\Psi}$. At $B = 0$, the minima at $\phi=0$, 1 are degenerate, and the ordered phase takes over at $B>0$, where $\phi\approx1$ becomes the global minimum. In the metastable regime $B<B_c=16g$, there exists a finite energy barrier between the two minima, whose strength is g right at the transition. The stiffness σ gives rise to a surface tension between domains of $\phi=0$ and $\phi\approx1$,

$$J_\phi = \int_0^{\phi_{>0}} d\phi \sqrt{2\sigma V(\phi)}, \tag{2}$$

where $V(\phi)=16g\phi^2(\phi-1)^2 - B\phi^2$, and $\phi_{>0}$ is the maximal ϕ for which $V(\phi)>0$. The correlation length is calculated by optimizing the energy of a domain-wall for $B=0$ (See Supplementary Section S1), $\xi_\phi = \sqrt{\frac{\sigma}{8g}}$.

In the second part of F, $a(r)$ is associated with the second-order transition. When $a>0$, the decoupled uniform solution is $|\Psi| = \Psi_0\sqrt{\frac{a}{b}}$.

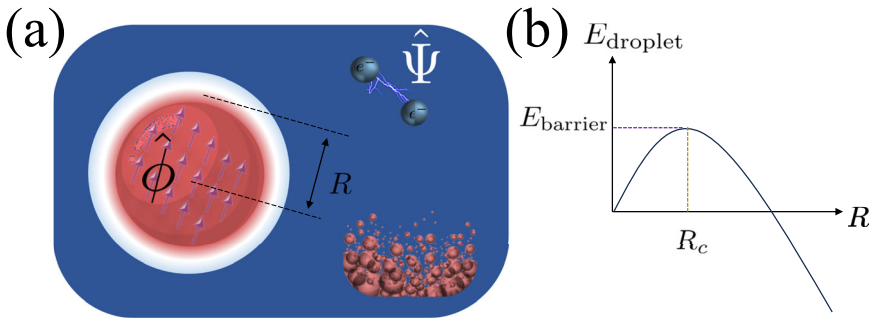

Fig. 2 | Critical droplet formation and analysis. a Illustration of a bubble of the true vacuum phase $\hat{\phi}$ (e.g., ferromagnet) within a metastable bulk $\hat{\Psi}$ phase (superconductor). Due to the incompatibility of the phases, there exists a narrow "corona" where $\hat{\Psi}$ is first suppressed, and only then $\hat{\phi}$ is established. **b** Schematic dependence of the bubble energy on its radius. Due to surface tension contributions, the droplet energy first increases with R, before eventually trending towards expansion. The critical radius R_c, as well as the threshold energy $E_{\text{thresh.}}$, are indicated.

Here the appropriate correlation (coherence) length is $\xi_\Psi = \sqrt{\kappa/(2a)}$, and the surface tension is $J_\Psi = \frac{8}{3}\xi_\Psi \frac{a^2}{4b}$. Finally, $\lambda > 0$ couples the two sectors, and precludes $\hat{\phi}$-$\hat{\Psi}$ order coexistence when it is sufficiently large as compared to the energy densities g and a.

We consider the system described by Eq. (1), initialized to the ordered (superconducting) Ψ_0 phase, yet tuned to metastability, $a > 0$ and $0 < B < B_c$. The true vacuum is $\phi \approx 1$, yet the initial state of the system is a locally stable minimum of the free energy. We schematically evaluate the characteristic time necessary for the system to decay to the true vacuum, adapting the methods developed by Langer[41] and Coleman[9].

Neglecting quantum fluctuations (whose role we later discuss), relaxation is facilitated by thermal fluctuations of $\hat{\phi}$ droplets (or "bounces"[1]) within the $\hat{\Psi}$ bulk, see illustration in Fig. 2a. The energy of a droplet with radius R may be evaluated in the so-called thin-wall limit ($R \gg \xi_\phi$) by refs. 1,9

$$\begin{aligned} E_{\text{droplet}} &= \pi R^2 f_{\text{true}} - \pi(R+\delta R)^2 f_{\text{meta}} \\ &+ 2\pi R J_\phi + 2\pi(R+\delta R) J_\Psi, \end{aligned} \tag{3}$$

where $f_{\text{true}} = -B$, $f_{\text{meta}} = -\frac{a^2}{4b}$, and $\delta R \approx \left(\xi_\phi + \xi_\Psi\right)/2$, due to the necessary suppression of the $\hat{\Psi}$ preceding the $\hat{\phi}$ droplet formation. The droplet experiences an effective force $\propto \partial E_{\text{droplet}}/\partial R$, pushing it towards either expansion or collapse, thus determining its fate. Thus, the droplet energy threshold, i.e., the droplet energy at which it would tend to overtake the system, will be given by

$$E_{\text{thresh.}} = E_{\text{droplet}}(R_c), \tag{4}$$

and

$$R_c = \frac{J_\phi + J_\Psi - \delta R f_{\text{meta}}}{f_{\text{meta}} - f_{\text{true}}}, \tag{5}$$

determined by $\partial E_{\text{droplet}}/\partial R|_{R_c} = 0$ (Fig. 2b). The expression for R_c accounts for two effects, which are *solely due to the ordered* $\hat{\Psi}$ *phase*, on top of the FV.

First, the denominator in Eq. (5) is made smaller by the presence of the finite condensation energy of $\hat{\Psi}$. In our regime of interest, as we discuss below, one usually finds $|f_{\text{true}}| \gg |f_{\text{meta}}|$, and this effect is of vanishing importance.

Second, the additional J_Ψ in the numerator, associated with the surface tension of the secondary (superconducting) phase, is reasonably expected to be rather small compared to J_ϕ, the surface tension contribution of the dominant correlated order, yet not negligible. This is because the surface tension is roughly proportional to the product of the correlation length and the energy scale associated with the ordered phase. While the latter might be much bigger for $\hat{\phi}$ as compared to $\hat{\Psi}$, this difference is usually somewhat compensated by the ration of correlation lengths, $\xi_\Psi \gg \xi_\phi$. In the regime where the denominator effect is negligible, one may approximate the threshold droplet radius $R_c \approx J_\phi / B\left(1 + cJ_\Psi/J_\phi\right)$, where c is an order-1 numerical factor which depends on microscopic details. As we demonstrate for the particular systems we consider below, this mechanism indeed facilitates a more stable false vacuum in the presence of the secondary $\hat{\Psi}$ phase, which in our case is a superconductor.

Our analysis utilizes the classical Ginzburg-Landau functional, Eq. (1), producing a free-energy barrier towards nucleation and eventual FV decay. Let us discuss the role of quantum fluctuations on the phenomenon described here. In the zero temperature limit, $\beta = \frac{1}{T} \to \infty$, any finite energy barrier completely annihilates decay through thermal fluctuations. However, fluctuations due to the quantum nature of the $\hat{\phi}$ field may overcome this limitation.

Setting aside $\hat{\Psi}$ for a moment, one interprets the $\hat{\phi}$ part of Eq. (1) as the classical limit of the imaginary-time action $S_\phi = \int_0^\beta d\tau \int d^d x \left[\frac{\rho}{2}(\partial_\tau \phi)^2 + \frac{g}{2}|\nabla\phi|^2 + V(\phi)\right]$. This corresponds to the imaginary-time path integral partition function $Z = \int D\phi e^{-S_\phi}$. In the $\rho \to \infty$ limit, variations along the τ dimension are suppressed, and one recovers the classical limit (with a prefactor of β replacing $\int d\tau$ integration).

Performing similar nucleation calculus in Euclidean space-time (see Supplementary Section S1), one finds a temperature scale, T_Q, below which the quantum decay pathway is dominant,

$$T_Q = \frac{3}{32}\frac{B\xi_\phi}{J_\phi}\tau_\phi^{-1}, \tag{6}$$

with $\tau_\phi = \sqrt{\frac{\rho}{8g}}$. We stress that below T_Q the FV phenomenon persists, yet the lifespan of the metastable phase *saturates* and remains roughly the same as the temperature is lowered further.

Notably, at any finite temperature, a small enough bias B exists such that the quantum decay is much less efficient. The reason for this dependence on the bias B stems from the effective higher dimension of the quantum problem, where the surface of the droplet is d-dimensional, whereas classically, it is $(d-1)$-dimensional. As a consequence (see Supplementary Section S1), the threshold energy scales as B^{-d} in the quantum case (B^{1-d} classically). Thus, when the bias between the false and true vacuum is small enough, the quantum decay pathway is highly disfavored. Without loss of generality, we henceforth assume this is the case for our detailed microscopic analysis below.

Another interesting possibility occurs in an intermediate temperature regime, where quantum behavior dominates the $\hat{\phi}$ sector, yet

$\hat{\Psi}$ (now introduced back in our discussion), remains effectively classical due to its much longer correlation time τ_ψ. The relevant temperature regime is $\frac{\tau_\phi}{\tau_\psi} < T/T_Q < 1$. Heuristically, it takes considerably lower temperatures (as compared to T_Q) to saturate the effects of the $\hat{\Psi}$ field redistribution energetics.

This regime thus enables further enhancement of the FV stability by the competing sub-leading order, as discussed in Supplementary Section S1. Once more, this enhancement takes place even if the discrepancy between f_{true} and f_{meta} is of orders of magnitude, due to combination of the correlation length effect $\xi_\psi \gg \xi_\phi$ (already discussed above) and a $\propto T_Q/T$ prefactor to the relative $\hat{\Psi}$ contribution. Thus, the lower the temperature in this regime, the larger the FV lifetime enhancement becomes due to the ordering competition.

Realization in graphene multilayers

We consider first-order phase boundaries observed in both BBG and RTG separating correlated symmetry-broken phases and superconductivity, either incipient or fully formed. In all cases, we follow the same methodology allowing us to extract the relevant energy densities and surface tensions.

We begin with a Hamiltonian of the form

$$H = H_0 + H_{\text{int}}, \tag{7}$$

where H_0 describes the appropriate band structure and $H_{\text{int}} = \frac{U_c}{\Omega}\sum_{\mathbf{q}}\rho_{\mathbf{q}}\rho_{-\mathbf{q}}$ is the electron-electron interaction, which we take as short-range for simplicity ($\rho_{\mathbf{q}}$ is the momentum-$\mathbf{q}$ component of the density in the relevant band, U_c is the interaction strength, and Ω is the system area). At a given density n_{tot}, we compute the free energy as a function of the relevant order parameter $\hat{\phi}$,

$$F(\phi) = \langle H\rangle_{\text{HF},(\phi,n_{\text{tot}})} - \langle H\rangle_{\text{HF},(0,n_{\text{tot}})}, \tag{8}$$

where $\langle\rangle_{\text{HF},(\phi,n)}$ is the Hartree-Fock expectation value for $\hat{\phi} = \phi$ at fixed density n. We use the zero-temperature expression, as the temperature is assumed to be far below the $\hat{\phi}$ phase transition. Contributions to Eq. (8) due to fluctuations around the mean-field solution, as well as due to other competing instabilities are beyond the current scope of this work.

As the energy scales associated with the order parameter jumps are comparable to the Fermi energy (see below) we will approximate the correlation length as the inter-particle separation, i.e., $\xi_\phi \approx n_{\text{tot}}^{-1/2}$. The stiffness is thus approximated by $\sigma \approx 8\xi_\phi^2 F^*$, with the barrier height $F^* = \max F(\phi \in [0, \phi_0])$. ϕ_0 is the global minima of F, and we approximate $B \approx -F(\phi_0)$.

In the normal state, we evaluate two crucial quantities regarding superconductivity. Namely, the critical temperature T_c, and the superconducting condensation energy, playing the role of $a^2/(4b)$ in our discussion above, Eq. (1). The superconducting coherence length is taken as a phenomenological parameter from experiments and assumed to scale with T_c in the conventional manner. The details of our superconducting calculations are presented in Supplementary Section S2, where we use general considerations and avoid making assumptions on the origin of the pairing glue. Moreover, we refrain from pinpointing the exact mechanisms by which the transition into the correlated phase extinguishes superconductivity and keep our discussion as general as possible. (In Supplementary Section S3 we discuss a curious scenario where the transition suppresses the superconducting phase through a combination of substantial DOS reconstruction and retardation effects.)

Intervalley coherence in rhombohedral trilayer graphene (RTG). A promising candidate to observe the phenomenon introduced here is the superconductor region denoted as SC1 in ref. 26. Its boundary in the n_{tot}–D plane (where D is the perpendicular displacement field) coincides with a transition to a symmetry-broken correlated phase, which appears to be first-order[26,37]. Though the nature of the correlated phase terminating SC1 has not been confirmed, it is somewhat constrained. The lack of spin and orbital ferromagnetism suggests either spin-valley locking, an intervalley-coherent phase (IVC), or a combination thereof. Theoretical studies have shown the IVC to be robust and ubiquitous throughout the phase diagram[42,43], steering our focus to the IVC case for simplicity.

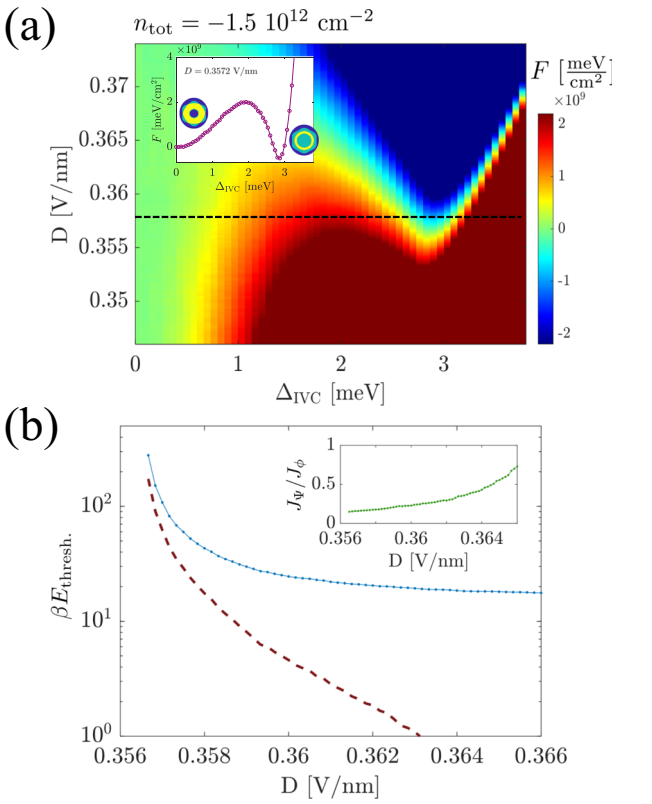

Fig. 3 | Ephemeral superconductivity near an IVC transition in RTG. a Free energy landscape for the IVC phase transition in RTG as a function of displacement field. A metastable regime is visible, where a free energy barrier separates an ordered minimum from the normal state. The fixed density is indicated. Inset: horizontal cut corresponding to the dashed black line in the main panel. The left and right circles are schematics of the Fermi surface in the normal and IVC phases, respectively. **b** The decay threshold energy in the vicinity of the transition (blue). The dashed purple line corresponds to the result in the absence of the superconductor. Inset: comparison of the surface tension contributions from the superconducting and IVC phases. The parameters used: $T = 30$ mK $U_C = 1.46$ eV nm^2, $g_{\text{att.}} = 0.21$ eV nm^2, $\omega^* = 0.5$ meV.

In Fig. 3a we plot the Hartree-Fock energy landscape as a function of the IVC order parameter and displacement field. Moving from low to high fields, one clearly observes a region of metastability: the global minimum is at ~3 meV, whilst the normal state remains locally stable. At high enough values of D, the normal state finally becomes unstable. We note in passing that in our Hartree-Fock calculations a similar region of metastability occurs when the displacement field as kept constant and the total density is varied, see Supplementary Section S3.

Next, we compute the false-vacuum decay threshold, shown in Fig. 3b. As expected, close to the transition point it diverges due to a vanishing energy difference between the FV and the true vacuum, driving the critical droplet size increasingly larger [Eq. (5)]. Notably, the threshold for decay becomes much smaller when the FV state is not superconducting, due to the surface tension contribution of the superconductor. As shown in the inset, the relative strength of J_ψ

increases, signaling two effects. The first is a decrease in the ordered phase surface tension J_ϕ [Eq. (2)] as the bias between the true and false vacuum increases. The second is a result of *enhanced superconductingT*$_c$, owing to an enhancement of DOS near the Fermi level as one moves deeper into the ordered state.

We now turn to estimate the lifetime of this false vacuum,

$$\tau_{\text{decay}} \sim \tau_0 e^{\beta E_{\text{thresh}}}, \tag{9}$$

where τ_0 is the much debated[7,10] fluctuation time-scale prefactor. For simplicity, we take the worst-case-scenario, and estimate it as the time two electrons separated by a correlation length can "know about each other", $\tau_0 \approx \xi_\phi/v_F \approx 10^{-13}$ sec. Taking a reasonable $\beta E_{\text{thresh.}} \sim 15$–$20$ leads to time scales $\tau_{\text{decay}} \sim O(100\,\text{nsec} - 10\,\mu\,\text{sec})$. For practical reasons, it is clear that τ_{decay} should far exceed the timescale over which the quench in the external parameter is realized. For the displacement field, the relevant timescale is the so-called RC charging time τ_{RC} associated with the dual-gate geometry. Using realistic device parameters, we estimate τ_{RC}<0.1nsec, orders of magnitude shorter than τ_{decay}. We note that the estimated decay lifetime (9) assumes a single-droplet picture, neglecting intriguing possibilities of multi-droplet false vacuum decay and true vacuum percolation. This assumption is justified in the cases discussed here, where characteristic device sizes on the $\sim\mu$m scale and are comparable to the typical size of the critical droplet R_c in the vicinity of the transition (see Supplementary Section S3).

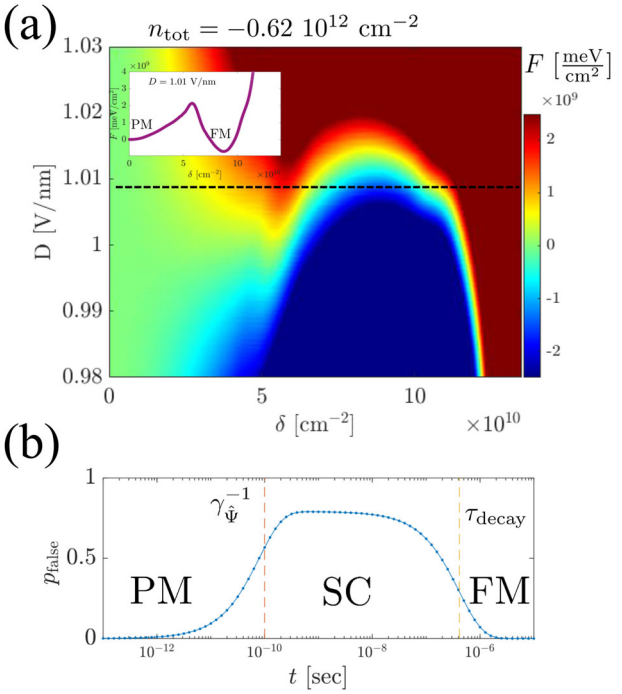

Fig. 4 | Ephemeral superconductivity near a Stoner transition in BBG. a Free energy landscape for the Stoner phase transition in BBG as a function of displacement field (the fixed density is indicated). Approaching the transition from the high D side, a metastable regime is reached. Inset: horizontal cut corresponding to the dashed black line in the main panel. **b** Occupation probability of the false vacuum superconductor evolving in time [Eq. (10)]. The system is initially in the FV paramagnetic state (PM), and superconductivity develops atop the metastable FV (SC), followed by an eventual decay to the equilibrium ferromagnet (FM). The characteristic superconductor formation time $\gamma_{\hat{\Psi}}^{-1}$ and decay time are indicated by horizontal red and yellow lines, respectively. The parameters used: $T = 30$ mK, $U_C = 1.8$ eV nm^2, $g_{\text{att.}} = 0.265$ eV nm^2, $\omega^* = 0.5$ meV, $t_{\text{decay}}/\tau_0 = e^{15}$, $\gamma_0^{-1}/\tau_0 = e^8$, $\gamma_{\hat{\Psi}}^{-1} = 100$ psec.

Stoner blockade in Bernal bilayer graphene (BBG). The phase diagram of BBG has been shown to host a multitude of sharp phase transitions, as well as superconductivity in the presence of either an in-plane magnetic field or proximity to WSe_2[27,28,37]. The phenomenology is suggestive of a vicinity of a superconductive phase in the absence of these two perturbations, where the formation of a competing correlated phase suppresses it refs. 44,45. We consider an alternative route to circumvent the presumed correlated phase, by quenching across the transition.

We focus on the vicinity of the magnetic-field-induced superconducting regime, where phenomenology is consistent with a four-fold to twofold degenerate Stoner transition. The Hartree-Fock free energy as a function of the polarization order parameter is shown in Fig. 4a. A metastable regime is clearly developed near the transition. The normal-state energetic are quite similar to those obtained for the RTG case, and lead to similar energy threshold, even when accounting for a lower T_c of the superconductor observed in experiments (see Supplementary Section S3).

There is a notable difference in this case compared to the RTG scenario above. Here, the system is in the normal state after the quench. It decays to the correlated phase with the characteristic τ_{decay}, yet superconductivity may form more rapidly, as it does not need to overcome an energy barrier. We estimate the superconductor formation rate as $\gamma_\Psi \sim \Delta_0$, i.e., roughly proportional to the equilibrium superconducting gap[46,47]. Combining the decay rate $\gamma = \tau_{\text{decay}}^{-1}$, γ_Ψ, and the decay rate in the absence of superconductivity γ_0, we may approximate the probability of the system being in the superconducting false vacuum (Supplementary Section S3),

$$p_{\text{false}}(t) = \frac{\gamma_{\hat{\Psi}}}{\gamma_{\hat{\Psi}} + \gamma_0 - \gamma}\left[1 - e^{-(\gamma_{\hat{\Psi}} + \gamma_0 - \gamma)t}\right] e^{-\gamma t}. \tag{10}$$

As demonstrated in Fig. 4b, at early times superconductivity builds up at a rate $\sim \gamma_{\hat{\Psi}}$ to some finite fraction and decays at long times at the rate γ. Our calculations indicate superconductivity should remain visible up to $O(100)$ nsec timescales.

In principle, for the specific scenario described in this section, where the system is quenched rapidly through a superconducting phase transition, one should take into account the formation of topological defects (vortices) due to the Kibble-Zurek mechanism[48,49]. Physically, one expects that following the quench, independently coherent domains of size $\sim\xi_\Psi$ form, and coalesce at a time-scale $\tau_{GL} \approx \pi/(8|T_c - T|)^{-1}$ [50,51], the Ginzburg-Landau relaxation time[52]. We note that τ_{GL} is of the same order of $\gamma_{\hat{\Psi}}^{-1}$. The relaxation dynamics of these defects, as well as oscillations in the order parameter magnitude[46] are presumed to play a secondary role and are thus beyond the current scope of this work.

Detecting ephemeral superconductivity

Thus far we have demonstrated the stabilization of the false vacuum by superconductivity, as well as the potential enhancement of the superconducting state in the metastable regime. We now explore another intriguing consequence of the physics studied in this work. Namely, the superconducting nature of the false vacuum makes the phenomenon readily accessible to transport measurements.

Consider an experimental setup similar to the one pioneered in ref. 53, depicted in the inset of Fig. 5. The tuning parameter in the system, e.g., displacement field, is quenched from time $-t_{\text{quench}}$ to $t = 0$. At $t = 0$ a current pulse is fed to the device, and the transient voltage response is recorded. At a time $t = t_{\text{delay}}$ voltage drop is eventually observed. originally, the experiment was tailored to measure the relaxation time of equilibrium superconductors, and thus no signal would appear if the amplitude of the current pulse is less than the superconducting critical current I_c. Here, the situation is made significantly richer by the decay of superconductivity itself.

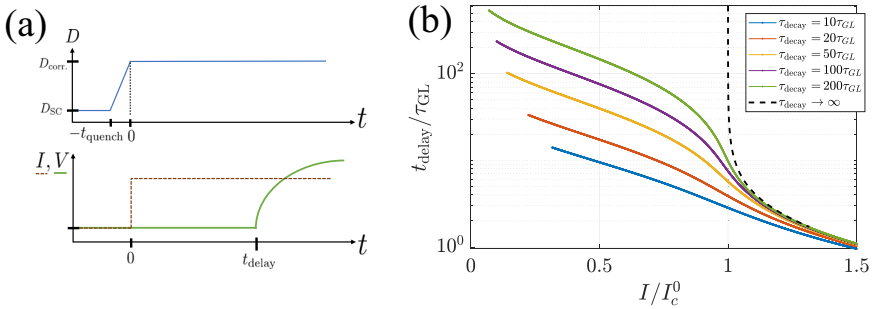

Fig. 5 | Measuring the order parameter relaxation dynamics. a A control parameter, e.g., D is quenched through the first-order phase transition (top). The quench duration is t_{quench}, and it ends at $t = 0$, at which time a current is driven through the system, and the time-resolved voltage signal is measured (bottom). **b** Calculations of the order parameter relaxation, performed by integrating Eq. (11) over time. Each curve is terminated at small currents at a value $I = I_c^0\sqrt{\frac{\tau_{GL}}{\tau_{decay}}}$, where we expect our simplified treatment to no longer be a good approximation (Supplementary Section S4).

Under some simple yet reasonable assumptions (see Supplementary Section S4), we find the delay as the time at which $f(t_{delay}) = 0$, with the initial conditions $f(0) = 1$, where f obeys the time evolution,

$$\tau_{GL}\partial_t f = -e^{2t/\tau_{decay}}\left(\frac{I}{I_c}\right)^2\frac{4}{27f^3} + f\left(1-f^2\right). \tag{11}$$

In Fig. 5 we demonstrate the dependence of the voltage signal delay time on the amplitude of the injected current. If the false vacuum state is stable enough, a noticeable uptick in the delay is made clearly visible for currents slightly below the equilibrium critical values. At relatively small values of the probe current, the expected delay is of the same order as the false-vacuum decay time τ_{decay}.

Discussion

Ephemeral superconductivity is a fascinating non-equilibrium state of matter, which is yet to be fully clarified[50,54–59]. Here, we explore an unusual striking phenomenon: Superconductivity developing on top of a correlated false-vacuum manifold. In contrast with previous scenarios where superconductivity is terminated by a first-order phase transition[60,61], the transient superconductor is temporarily protected by the correlated FV. Furthermore, the FV can facilitate the formation of a superconductor followed bu its decay (Fig. 4b), in otherwise superconductivity-excluded areas of the equilibrium phase diagram. The proposed non-equilibrium superconductor is incompatible with the true many-body ground state of the system and is thus ephemeral albeit metastable.

We elucidated how this FV superconductor can remarkably and significantly *enhance the false-vacuum lifespan*, possibly by a few orders of magnitude. This enhancement occurs even if the superconducting condensation energy is negligible as compared to that of the correlated true vacuum, as we demonstrated by utilizing a general phenomenological framework [Eq. (1)]. This unique effect is rooted in a notable surface tension contribution of the superconductor to the nucleation of critical threshold droplets, which facilitates the decay[1,9,41]. The prospect of FV stabilization by a generic secondary order, which is adversarial to the corresponding true vacuum, is left for future work, as well as a broader view of quantum effects and the hybrid quantum-classical regime.

We demonstrated how the ephemeral superconducting state can be realized in multilayer graphene devices. These systems ubiquitously show the coexistence of superconducting regions in the phase diagram, and apparent first-order phase transitions to correlated symmetry-broken phases[25,35–38]. On occasions, these transitions actually terminate the superconducting dome, making such devices an ideal platform to explore the intertwined false-vacuum physics. Combining Hartree-Fock calculations for the symmetry-broken transition energetics, theory of the superconductivity transition, and phenomenology obtained from experiments, we estimate the relevant FV lifetime for observing the FV decay to be $\gtrsim O(100\,\text{nsec})$, rendering the decay process as much slower as compared to recently observed transient superconducting phenomena[59,62–65].

Another intriguing prospect in these graphene systems is that competition with a correlated phase transition arguably undermines the potential equilibrium superconducting orders. (This is reminiscent of the competing phases in high-T_C superconductors, e.g., ref. 66.) The multilayer graphene superconductors were observed to be stabilized by some perturbations, e.g., magnetic fields or proximity to a non-trivial substrate. However, we have pointed out a different route for bringing these low-lying superconductors to light: transiently suppressing the symmetry-broken state by quenching the system through the first-order transition. The motivation for such a process to be feasible is simple. The same factor that participates in driving the transitions, the DOS near the Fermi energy, is the one that is expected to enhance superconductivity when given the chance (see related discussion in refs. 45,67).

An important consequence of ephemeral superconductivity "dressing" the metastable false vacuum is that direct experimental detection of its decay becomes simple and experimentally accessible. The long time scales for the superconducting life-times mentioned above are, in fact, conducive to straightforward transport measurements. Resolution of ~1 nsec in the voltage-delay experimental scheme we detail in Sec. can readily be obtained. Tracking the temporal signal due to the decay of the superconductor and, as a consequence, the establishment of the equilibrium ground-state may be achieved in these graphene systems (as well as in another candidate system, twisted WSe_2[40]), without the need of sophisticated light-based apparatus. Moreover, conclusive transport signatures of the kind we discussed obviate many of the ambiguities associated with photo-measurements of non-equilibrium superconductors[68]. These facts, along with the ability to electrically tune them across the phase diagram, make highly correlated multilayer graphene devices ideal playgrounds for manipulating and probing the false-vacuum decay in the context of solid-state systems.

Data availability

The data supporting the findings in this work are publicly available online at https://doi.org/10.5281/zenodo.14290558.

Code availability

The code used to generate the data and figures appearing in this work is available online at https://github.com/galshavit/EphemeralSC.

References

1. Altland, A. & Simons, B. D. *Condensed Matter Field Theory* (Cambridge University Press, 2010).
2. Wen, X.-G. *Quantum Field Theory of Many-Body Systems: From the Origin of Sound to an Origin of Light and Electrons* (OUP Oxford, 2004).
3. Debenedetti, P. G. *Metastable Liquids: Concepts and Principles*, vol. 1 (Princeton University Press, 1996).
4. Rutkevich, S. B. Decay of the metastable phase in $d = 1$ and $d = 2$ ising models. *Phys. Rev. B* **60**, 14525–14528 (1999).
5. Lagnese, G., Surace, F. M., Kormos, M. & Calabrese, P. False vacuum decay in quantum spin chains. *Phys. Rev. B* **104**, L201106 (2021).
6. Milsted, A., Liu, J., Preskill, J. & Vidal, G. Collisions of false-vacuum bubble walls in a quantum spin chain. *PRX Quantum* **3**, 020316 (2022).
7. McCumber, D. E. & Halperin, B. I. Time scale of intrinsic resistive fluctuations in thin superconducting wires. *Phys. Rev. B* **1**, 1054–1070 (1970).
8. Zenesini, A. et al. False vacuum decay via bubble formation in ferromagnetic superfluids. *Nat. Phys.* **20**, 558–563 (2024).
9. Coleman, S. Fate of the false vacuum: Semiclassical theory. *Phys. Rev. D* **15**, 2929–2936 (1977).
10. Callan, C. G. & Coleman, S. Fate of the false vacuum. ii. first quantum corrections. *Phys. Rev. D* **16**, 1762–1768 (1977).
11. Turner, M. S. & Wilczek, F. Is our vacuum metastable? *Nature* **298**, 633–634 (1982).
12. Cao, Y. et al. Correlated insulator behaviour at half-filling in magic-angle graphene superlattices. *Nature* **556**, 80–84 (2018).
13. Cao, Y. et al. Unconventional superconductivity in magic-angle graphene superlattices. *Nature* **556**, 43–50 (2018).
14. Lu, X. et al. Superconductors, orbital magnets and correlated states in magic-angle bilayer graphene. *Nature* **574**, 653–657 (2019).
15. Hao, Z. et al. Electric field-tunable superconductivity in alternating-twist magic-angle trilayer graphene. *Science* **371**, 1133–1138 (2021).
16. Park, J. M., Cao, Y., Watanabe, K., Taniguchi, T. & Jarillo-Herrero, P. Tunable strongly coupled superconductivity in magic-angle twisted trilayer graphene. *Nature* **590**, 249–255 (2021).
17. Park, J. M. et al. Robust superconductivity in magic-angle multilayer graphene family. *Nat. Mater.* **21**, 877–883 (2022).
18. Zhang, Y. et al. Promotion of superconductivity in magic-angle graphene multilayers. *Science* **377**, 1538–1543 (2022).
19. Shen, C. et al. Correlated states in twisted double bilayer graphene. *Nat. Phys.* **16**, 520–525 (2020).
20. Cao, Y. et al. Tunable correlated states and spin-polarized phases in twisted bilayer–bilayer graphene. *Nature* **583**, 215–220 (2020).
21. Liu, X. et al. Tunable spin-polarized correlated states in twisted double bilayer graphene. *Nature* **583**, 221–225 (2020).
22. Kuiri, M. et al. Spontaneous time-reversal symmetry breaking in twisted double bilayer graphene. *Nat. Commun.* **13**, 6468 (2022).
23. Su, R., Kuiri, M., Watanabe, K., Taniguchi, T. & Folk, J. Superconductivity in twisted double bilayer graphene stabilized by wse2. *Nat. Mater.* **22**, 1332–1337 (2023).
24. Uri, A. et al. Superconductivity and strong interactions in a tunable moiré quasicrystal. *Nature* **620**, 762–767 (2023).
25. Zhou, H. et al. Half- and quarter-metals in rhombohedral trilayer graphene. *Nature* **598**, 429–433 (2021).
26. Zhou, H., Xie, T., Taniguchi, T., Watanabe, K. & Young, A. F. Superconductivity in rhombohedral trilayer graphene. *Nature* **598**, 434–438 (2021).
27. Zhou, H. et al. Isospin magnetism and spin-polarized superconductivity in bernal bilayer graphene. *Science* **375**, 774–778 (2022).
28. Zhang, Y. et al. Enhanced superconductivity in spin–orbit proximitized bilayer graphene. *Nature* **613**, 268–273 (2023).
29. Seiler, A. M. et al. Quantum cascade of correlated phases in trigonally warped bilayer graphene. *Nature* **608**, 298–302 (2022).
30. Li, C. et al. Tunable superconductivity in electron- and hole-doped bernal bilayer graphene. *Nature* **631**, 300–306 (2024).
31. Han, T. et al. Orbital multiferroicity in pentalayer rhombohedral graphene. *Nature* **623**, 41–47 (2023).
32. Han, T. et al. Correlated insulator and chern insulators in pentalayer rhombohedral-stacked graphene. *Nat. Nanotechnol.* **19**, 181–187 (2024).
33. Liu, K. et al. Spontaneous broken-symmetry insulator and metals in tetralayer rhombohedral graphene. *Nat. Nanotechnol.* **19**, 188–195 (2024).
34. Lu, Z. et al. Fractional quantum anomalous hall effect in multilayer graphene. *Nature* **626**, 759–764 (2024).
35. Yang, J. et al. Diverse impacts of spin-orbit coupling on superconductivity in rhombohedral graphene. Preprint at https://arxiv.org/abs/2408.09906 (2024).
36. Zhang, Y. et al. Twist-programmable superconductivity in spin-orbit coupled bilayer graphene. Preprint at https://arxiv.org/abs/2408.10335 (2024).
37. Holleis, L. et al. Nematicity and orbital depairing in superconducting Bernal bilayer graphene. *Nat. Phys.* https://doi.org/10.1038/s41567-024-02776-7 (2025).
38. Patterson, C. L. et al. Superconductivity and spin canting in spin-orbit proximitized rhombohedral trilayer graphene. Preprint at https://arxiv.org/abs/2408.10190 (2024).
39. Choi, Y. et al. Electric field control of superconductivity and quantized anomalous hall effects in rhombohedral tetralayer graphene. Preprint at https://arxiv.org/abs/2408.12584 (2024).
40. Guo, Y. et al. Superconductivity in twisted bilayer wse_2. Nature **637**, 833–838 (2024).
41. Langer, J. Theory of the condensation point. *Ann. Phys.* **41**, 108–157 (1967).
42. You, Y.-Z. & Vishwanath, A. Kohn-luttinger superconductivity and intervalley coherence in rhombohedral trilayer graphene. *Phys. Rev. B* **105**, 134524 (2022).
43. Koh, J. M., Alicea, J. & Lantagne-Hurtubise, E. Correlated phases in spin-orbit-coupled rhombohedral trilayer graphene. *Phys. Rev. B* **109**, 035113 (2024).
44. Dong, Z., Chubukov, A. V. & Levitov, L. Transformer spin-triplet superconductivity at the onset of isospin order in bilayer graphene. *Phys. Rev. B* **107**, 174512 (2023).
45. Shavit, G. & Oreg, Y. Inducing superconductivity in bilayer graphene by alleviation of the stoner blockade. *Phys. Rev. B* **108**, 024510 (2023).
46. Barankov, R. A. & Levitov, L. S. Synchronization in the bcs pairing dynamics as a critical phenomenon. *Phys. Rev. Lett.* **96**, 230403 (2006).
47. Pekker, D. et al. Competition between pairing and ferromagnetic instabilities in ultracold fermi gases near feshbach resonances. *Phys. Rev. Lett.* **106**, 050402 (2011).
48. Kibble, T. Some implications of a cosmological phase transition. *Phys. Rep.* **67**, 183–199 (1980).
49. Zurek, W. H. Cosmological experiments in superfluid helium? *Nature* **317**, 505–508 (1985).
50. Kopnin, N.*Theory of Nonequilibrium Superconductivity*. (Oxford University Press, 2001).
51. Weiler, C. N. et al. Spontaneous vortices in the formation of bose–einstein condensates. *Nature* **455**, 948–951 (2008).
52. Larkin, A. & Varlamov, A.*Theory of Fluctuations in Superconductors*. vol. 127 (OUP Oxford, 2005).
53. Pals, J. & Wolter, J. Measurement of the order-parameter relaxation in superconducting al-strips. *Phys. Lett. A* **70**, 150–152 (1979).

54. Galitskii, V., Elesin, V. & Kopaev, Y. V. Feasibility of high-temperature superconductivity in nonequilibrium systems with repulsion. *JETP Lett.* **18**, 27 (1973).
55. Elesin, V. F. & Kopaev, Y. V. Superconductors with excess quasiparticles. *Sov. Phys. Usp.* **24**, 116 (1981).
56. Galitski, V. M. & Larkin, A. I. Spin glass versus superconductivity. *Phys. Rev. B* **66**, 064526 (2002).
57. Goldstein, G., Aron, C. & Chamon, C. Photoinduced superconductivity in semiconductors. *Phys. Rev. B* **91**, 054517 (2015).
58. Raines, Z. M., Stanev, V. & Galitski, V. M. Enhancement of superconductivity via periodic modulation in a three-dimensional model of cuprates. *Phys. Rev. B* **91**, 184506 (2015).
59. Fausti, D. et al. Light-induced superconductivity in a stripe-ordered cuprate. *Science* **331**, 189–191 (2011).
60. Bianchi, A. et al. First-order superconducting phase transition in $CeCoIn_5$. *Phys. Rev. Lett.* **89**, 137002 (2002).
61. Yonezawa, S., Kajikawa, T. & Maeno, Y. First-order superconducting transition of sr_2ruo_4. *Phys. Rev. Lett.* **110**, 077003 (2013).
62. Hunt, C. R. et al. Two distinct kinetic regimes for the relaxation of light-induced superconductivity in $La_{1.675}Eu_{0.2}Sr_{0.125}Cuo_4$. *Phys. Rev. B* **91**, 020505 (2015).
63. Mitrano, M. et al. Possible light-induced superconductivity in k3c60 at high temperature. *Nature* **530**, 461–464 (2016).
64. Isoyama, K. et al. Light-induced enhancement of superconductivity in iron-based superconductor fese0.5te0.5. *Commun. Phys.* **4**, 160 (2021).
65. Rowe, E. et al. Resonant enhancement of photo-induced superconductivity in k3c60. *Nat. Phys.* **19**, 1821–1826 (2023).
66. Chang, J. et al. Direct observation of competition between superconductivity and charge density wave order in yba2cu3o6.67. *Nat. Phys.* **8**, 871–876 (2012).
67. Shavit, G., Berg, E., Stern, A. & Oreg, Y. Theory of correlated insulators and superconductivity in twisted bilayer graphene. *Phys. Rev. Lett.* **127**, 247703 (2021).
68. Dai, Z. & Lee, P. A. Superconducting like response in a driven gapped bosonic system. *Phys. Rev. B* **104**, 054512 (2021).

Acknowledgements

We thank John Curtis, Thomas Weitz, Dmitry Abanin, and Erez Berg for enlightening discussions. S.N.-P. acknowledges support from the National Science Foundation (grant number DMR-1753306). G.R. and S.N.-P. also acknowledge the support of the Institute for Quantum Information and Matter, an NSF Physics Frontiers Center (PHY-2317110). G.S. acknowledges support from the Walter Burke Institute for Theoretical Physics at Caltech, and from the Yad Hanadiv Foundation through the Rothschild fellowship. Part of this work was done at the Aspen Center for Physics, which is supported by the NSF grant PHY-1607611.

Author contributions

G.S. and G.R. conceived the idea for this project. G.S., S.N.-P., and G.R. performed research, analyzed data and calculation results, and wrote the manuscript.

Competing interests

The authors declare no competing interests.

Additional information

Supplementary information The online version contains supplementary material available at https://doi.org/10.1038/s41467-025-57227-5.

Correspondence and requests for materials should be addressed to Gal Shavit.

Peer review information *Nature Communications* thanks Wei Qin, and the other anonymous reviewer(s) for their contribution to the peer review of this work. A peer review file is available.